 FDMP, vol.7, no.3, pp.317-328, 2011

Viscoelastic Drop Deformation in a Micro-Contraction

Malcolm R. Davidson[1] **and Dalton J.E. Harvie**[1]

Abstract: A volume-of-fluid numerical method, adapted by the authors [Harvie, Cooper-White and Davidson (2008)] to simulate the flow of viscoelastic fluids, is used to predict deformation of a viscoelastic droplet carried by an immiscible Newtonian liquid through an axisymmetric microfluidic contraction-expansion. Values of the capillary number and elasticity number are chosen based on corresponding values for a rectangular contraction for which a reentrant cavity at the rear of the drop and subsequent encapsulation behaviour was observed experimentally by Harvie, Cooper-White and Davidson (2008). A reentrant cavity, similar to the observed one, is predicted; however, encapsulation is not achieved. Unexpectedly, a narrow cavity at the centre of the forward face of the drop exiting the contraction is also predicted for low capillary number and high elasticity number. The forward cavity eventually completely penetrates the drop so that it forms a torus.

Keywords: Volume-of-Fluid, contraction-expansion, microfluidics, viscoelastic, drop deformation.

1 Introduction

The increasing use of microfluidic devices in applications for biotechnology and research purposes often involves the production and movement of droplets in microchannels. Furthermore, a knowledge of droplet deformation within micron-sized channels is required for the optimum development of many products within the food, cosmetic, and photographic industries that use emulsions. Many fluids processed in microfluidic devices are viscoelastic. Examples include biological fluids such as DNA and protein suspensions, and fluids with small amounts of dissolved polymer.

Numerical methods capable of simulating multiphase viscoelastic flows with interfaces have evolved in the last 5-10 years since the early study by Keunings (1986) who used finite elements on a deforming mesh. Although there is some use of

[1] The University of Melbourne, Department of Chemical and Biomolecular Engineering, Melbourne, Australia

boundary-fitted meshes [Ramaswamy and Leal (1999); You, Borhan and Haj-Hariri (2008)], most modern techniques for simulating viscoelastic drop deformation are based on a stationary Eulerian grid. These include level-set [Pillapakkam and Singh (2001)], Volume-of-Fluid [Davidson, Harvie and Cooper-White (2006); Khismatullin, Renardy and Renardy (2006); Harvie, Cooper-White and Davidson (2008); Verhulst, Cardinaels, Moldenaers, Renardy and Afkhami (2009)], front tracking [Chung, Hulsen, Kim, Ahn and Lee (2008); Aggarwal and Sarkar (2008)], Marker-and-Cell [Tome, Doricio, Castelo, Cuminato and McKee (2007a); Tome, Grossi, Castelo, Cuminato, McKee and Walters (2007b)] and phase-field [Zhou, Yue, Feng, Ollivier-Gooch and Hu (2010)].

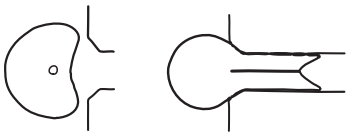

Figure 1: Schematic showing the long narrow rear cavity formation in a drop, and subsequent encapsulation of surrounding liquid, observed experimentally by Harvie, Cooper-White and Davidson (2008) for a drop passing through a rectangular contraction-expansion microchannel.

In recent years, the authors have been studying numerically the deformation of Newtonian and non-Newtonian droplets in flow through microchannels that are cylindrical or planar 4:1:4 contraction-expansions [Harvie, Davidson, Cooper-White and Rudman (2006); Harvie, Davidson, Cooper-White and Rudman (2007); Harvie, Cooper-White and Davidson (2008)]. A Volume-of-Fluid (VOF) numerical method was used. In the authors' study of viscoelastic drops [Harvie, Cooper-White and Davidson (2008)] they compared predictions of two-dimensional planar simulations with experimental results that exhibited some interesting behaviour caused by elastic stresses created at the rear of the drop as it passed through the contraction. In particular, the flow visualisation showed the development of a long and narrow reentrant cavity at the rear of the droplet followed by the encapsulation of a small amount of the surrounding liquid within the droplet (Fig. 1). However, although the simulations of Harvie, Cooper-White and Davidson (2008) predicted a reentrant cavity, and demonstrated the viscoelastic mechanism leading to the cavity and encapsulation, these features were poorly resolved. It is likely that a full three dimensional simulation at very high resolution is required to capture these very small scale effects in that case. The aim of this paper is to further study these effects, but without the computational penalty of a high resolution three dimensional viscoelastic calculation. We consider an axisymmetric cylindrical geometry with capillary

number (Ca) and elasticity number (El) chosen so that corresponding values based on velocity and radius in the contraction are similar to those in the planar contraction of Harvie, Cooper-White and Davidson (2008). Predictions for a range of values of Ca and El are then compared and discussed. The Oldroyd-B rheological model is used to represent the viscoelastic behaviour, and the VOF-based numerical scheme, described by Harvie, Cooper-White and Davidson (2008) for viscoelastic two-fluid flow, is used.

2 Formulation

Consider a droplet of viscoelastic liquid carried by an immiscible Newtonian liquid in axisymmetric flow through a circular cylindrical contraction. Figure 2 shows the details of the geometry where all lengths are scaled by the inlet radius R. The mean velocity of the liquid entering the inlet is denoted by $\overline{V}$. The dimensions in the generating plane of the cylindrical geometry are taken to be the same as those of the planar geometry considered by Harvie, Cooper-White and Davidson (2008). Consequently, in terms of scaled lengths, the initial droplet diameter $d = 0.864$, the contraction radius is 0.209, the length of the contraction and inlet regions are 5.364 and 3, respectively, while the total length of the flow domain is 12.

Viscoelastic fluids are typically polymeric solutions and rheological models such as the Oldroyd-B model (used here) are based on a representation of the polymer as an assembly of dumbbells. The polymer configuration is represented by the configuration tensor $\mathrm{A} = \langle \mathrm{RR} \rangle$ where R is the dumbbell end-to-end vector normalised by its magnitude at equilibrium, and $\langle \mathrm{RR} \rangle$ is an ensemble average.

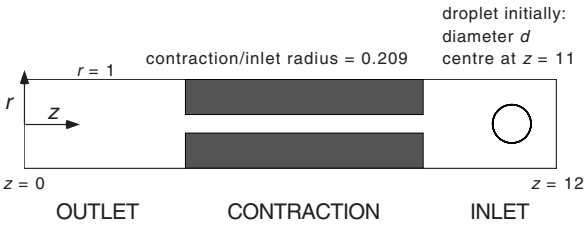

Figure 2: Schematic of the cylindrical flow geometry. All lengths are nondimensionalised by the inlet region radius and take values from the corresponding planar geometry described by Harvie, Cooper-White and Davidson (2008). The contraction corners are actually 'bevelled' slightly (not shown).

In terms of dimensionless velocity, length and time, scaled according to $\overline{V}$, R and $R/\overline{V}$, respectively, the equations of motion for a VOF calculation, that include vis-

coelastic effects, are

$$\frac{\partial \phi}{\partial t} + \nabla \cdot (\mathrm{U}\phi) = 0 \tag{1}$$

$$\frac{\partial \rho \mathrm{U}}{\partial t} + \nabla \cdot (\rho \mathrm{UU}) = -\nabla P + \frac{1}{\mathrm{We}} \mathrm{F_S} + \frac{1}{\mathrm{Re}} \nabla \cdot \tau \tag{2}$$

$$\nabla \cdot \mathrm{U} = 0 \tag{3}$$

$$\frac{\partial \mathrm{A}}{\partial t} + \mathrm{U} \cdot \nabla \mathrm{A} = \mathrm{A} \cdot \nabla \mathrm{U} + (\nabla \mathrm{U})^{\mathrm{T}} \cdot \mathrm{A} - \frac{1}{\mathrm{De}} (\mathrm{A} - \mathrm{I}) \tag{4}$$

$$\tau = \mu \left(\nabla \mathrm{U} + (\nabla \mathrm{U})^{\mathrm{T}} \right) + \frac{\mu_p}{\mathrm{De}} (\mathrm{A} - \mathrm{I}) \tag{5}$$

where ϕ is a fractional volume function, P is the fluid pressure, τ is a combined viscous and elastic stress tensor, $\mathrm{F_S}$ is the surface force arising from interfacial effects, and μ_p measures the polymer viscosity. The effect of gravity is ignored as it is negligible in microfluidics. The fractional volume function ϕ is advected with the local velocity U. The density (ρ) and solvent shear viscosity (μ) are scaled by their values for the continuous phase. Consequently, $\rho = \rho_d/\rho_c$ and $\mu = \mu_d/\mu_c$ inside the drop and $\rho = 1$, $\mu = 1$ within the continuous phase: in cells spanning the interface ρ and μ are taken to be averages, weighted by volume fraction. Subscripts c and d denote continuous phase and drop phase, respectively. The polymer viscosity (μ_p) is defined as the increase in shear viscosity over that of the solvent caused by the addition of the polymer, scaled by μ_c; i.e. it is a polymer contribution to the dimensionless shear viscosity.

The dimensionless parameters in Equations 1–5 are the Weber, Reynolds and Deborah numbers respectively:

$$\mathrm{We} = \frac{\rho_c \overline{V}^2 R}{\sigma}, \quad \mathrm{Re} = \frac{\rho_c \overline{V} R}{\mu_c}, \quad \mathrm{De} = \frac{\overline{V} t_p}{R}. \tag{6}$$

where σ is the coefficient of interfacial tension, and t_p is the polymer relaxation time.

3 Numerical Considerations

Equations 1–3 are solved using a finite volume method, combined with volume tracking, with explicit timestepping as developed by Rudman (1998) for Newtonian fluids. The algorithm used to solve equation 4 for the conformation tensor A is described in detail by Harvie, Cooper-White and Davidson (2008). One feature of the procedure is that the advection update of A during a timestep uses the volume fluxes of each phase that are determined by the VOF technique. This prevents

polymer from unphysically crossing the drop surface, and ensures that the diagonal components of A, and its determinant, remain positive as required physically. Another feature of the solution method for A is that the corresponding source update is performed implicitly to ensure solution stability.

Initially the drop and carrier liquid are assumed to be at rest. At $t > 0$ the fluid is assumed to enter with a fully developed Poiseuille velocity profile. However, the choice of entry velocity profile is not expected to be important for the low Reynolds numbers encountered in micro-channel flow. All computation domain walls are taken to be non-slip and also non-wetting with respect to the drop liquid.

The domain is discretised using uniform square cells in a staggered mesh with 128 cells spanning the inlet radius (a 128×1536 mesh). The volume function ϕ is solved on a mesh that is twice as fine (256×3072) as that used for the flow field. Grid sensitivity tests by Harvie, Cooper-White and Davidson (2008) quantified the effect of increasing the mesh density by considering 32×384, 64×768 and 128×1536 meshes for the flow field. They found a convergence in deformed droplet dimensions and shape with increasing mesh density. They also found that the best correspondence with experiment was obtained with the finest grid.

4 Results and Discussion

The fluid properties chosen for the simulations in this paper are the same as those used by Harvie, Cooper-White and Davidson (2008). Specifically, we choose $\rho_d/\rho_c = 1.17$, $\mu_d/\mu_c = 0.182$ and $\mu_p = 0.128$ in all simulations.

For the base case, the capillary number ($\mathrm{Ca} = \mathrm{We}/\mathrm{Re}$) and elasticity number ($\mathrm{El} = \mathrm{De}/\mathrm{Re}$) are chosen so that corresponding values based on velocity and radius in the cylindrical contraction are approximately the same as those in the planar contraction considered by Harvie, Cooper-White and Davidson (2008). Consistent with this, we set $\mathrm{Re} = 1.031$, $\mathrm{We} = 0.0194$ and $\mathrm{De} = 0.7475$ for the base case, for which $\mathrm{Ca} = 0.019$ and $\mathrm{El} = 0.725$. Simulations are performed for the base case and for surrounding values of capillary and elasticity number.

Figure 3 shows the evolution of drop shape when $\mathrm{Ca} = 0.019$ for varying elasticity number. The base case occurs for $\mathrm{El} = 0.725$ in this figure. Each case shows the formation of a long reentrant cavity at the rear of the drop, more like the experimentally observed one for rectangular channels (Fig. 1) than the shallow cavity predicted by the planar calculations of Harvie, Cooper-White and Davidson (2008). Encapsulation of continuous phase is almost achieved in the contraction, but the cavity eventually fails to completely close over. The differences with changing elasticity are small: the drop within the contraction at $t = 0.92$ is slightly longer when $\mathrm{El} = 0.145$ than it is when $\mathrm{El} = 0.725$ or 3.625. Also the drop emerging

from the contraction develops a very narrow cavity at the centre of the forward face of the drop at the larger values of El. The reason for this forward cavity will be discussed later in this section. No forward cavity was observed in the experiment reported by Harvie, Cooper-White and Davidson (2008).

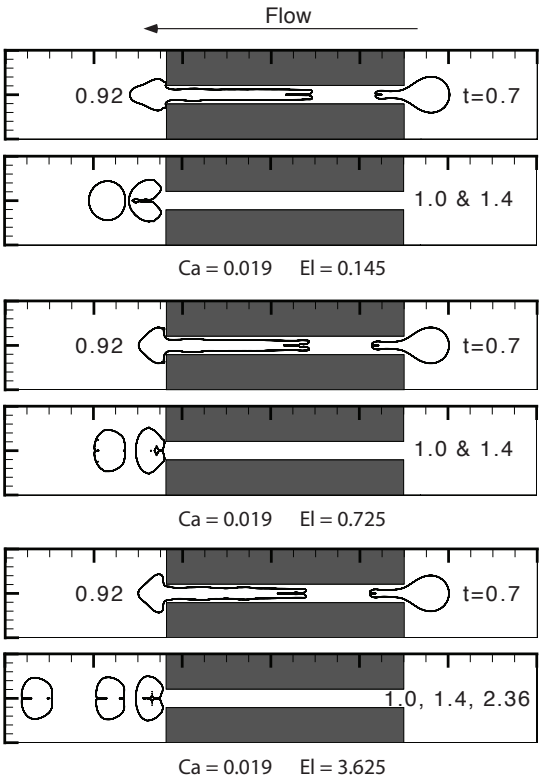

Figure 3: Predicted drop deformation at selected dimensionless times t for varying El when Ca $= 0.019$. The result for El $= 0.725$ is base case.

Figure 4 shows the evolution of drop shape when El $= 0.725$ for varying capillary number. The base case occurs for Ca $= 0.019$ in this figure. When the capillary number is reduced to 0.0038, the progress of the drop through the contraction is reduced and the length of the reentrant cavity at the rear is increased. Both of these effects occur because, at reduced capillary number, the importance of interfacial tension is increased so that the drop occupies more of the contraction width to reduce interfacial area. Because the drop surface is now closer to the wall of the contraction, friction on the drop is increased. The increased friction not only slows the progress of the drop in the contraction, but also increases polymer stretching

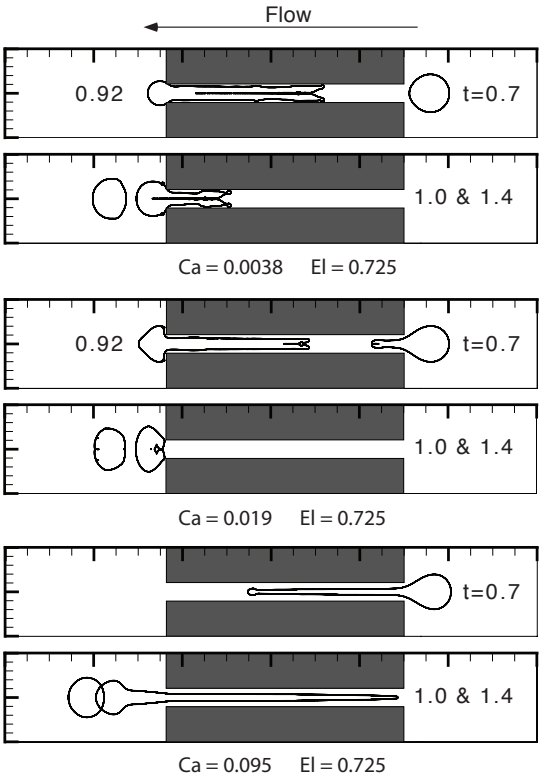

Figure 4: Predicted drop deformation at selected dimensionless times t for varying Ca when El $= 0.725$. The result for Ca $= 0.019$ is base case.

in the viscoelastic drop that, in turn, promotes the formation of the rear cavity as discussed by Harvie, Cooper-White and Davidson (2008). The converse occurs when Ca is increased from 0.019 to 0.095; in that case the effect of interfacial tension is reduced, so that the drop surface is further from the contraction wall, thus reducing friction on the drop so that the reentrant cavity does not form.

The results in Fig. 3 for Ca $= 0.019$ show the formation of a narrow cavity at the *forward* face of the drop when elasticity number is greatest (El $= 3.625$). This effect does not occur for the larger capillary number Ca $= 0.095$. Figure 5 shows that the forward cavity is more pronounced for El $= 3.625$ when the capillary number is smaller (Ca $= 0.0038$). At the largest time $t = 2.36$ the cavity has completely penetrated the drop so that it forms a torus. As before, the forward cavity is absent at the lowest value of elasticity number (El $= 0.145$).

The development of a cavity in the forward face of the drop can be explained with

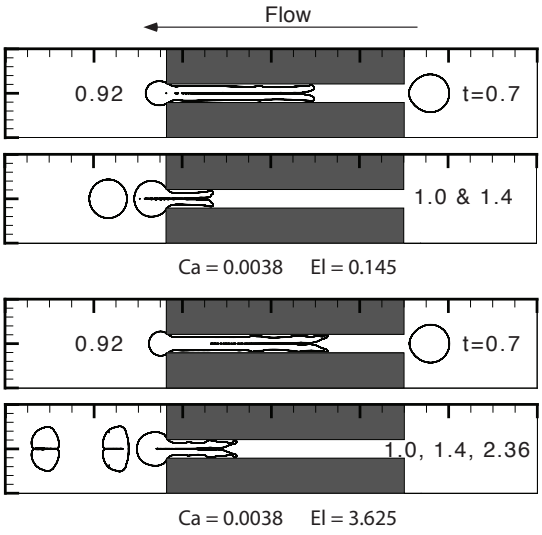

Figure 5: Predicted drop deformation at selected dimensionless times t for El = 0.145 and 3.625 when Ca = 0.0038.

reference to Fig. 6 for the lowest capillary number (Ca = 0.0038) and highest elasticity number (El = 3.625). In this somewhat magnified view of the drop exiting the contraction, the bevelled corners on the contraction are shown. The large arrowheads indicate the direction of flow within the drop. At $t = 1.0$, the elastic stress is high along the axis of symmetry in a region extending from the contraction to almost halfway into the drop (dark shaded region along the axis). This high stress is associated with the formation of the rear cavity (Fig. 4) as discussed by Harvie, Cooper-White and Davidson (2008). The effect of this elastic stress on the drop fluid emerging from the contraction is to drive the fluid near the centre of the drop back towards the contraction. This imparts a recirculation within the drop. The force driving this recirculation continues while drop fluid having high elastic stress remains inside the contraction. By the time the drop has completely exited the contraction at $t = 1.1$, the recirculation has strengthened significantly.

At $t = 1.1$, the flow at the forward face of the drop is converging towards the centreline, the elastic stress grows at the forward section, as is evident by the increased shading in this region. This elastic stress, in turn, reduces the centreline flow towards the rear of the drop and, at $t = 1.14$, has reversed the flow direction. The flow at the *rear* of the drop is now converging towards the centreline which increases the elastic stress at the rear section as well. At time $t = 1.3$, a thin band of elastic stress has developed along the entire axis of the drop (no forward cavity has formed yet).

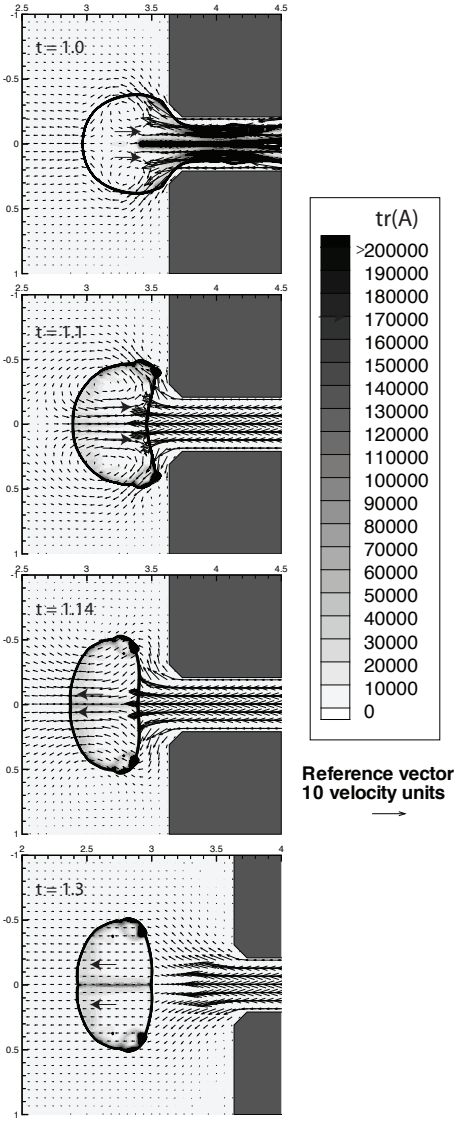

Figure 6: Predicted drop deformation and velocity field on exit from the contraction at selected dimensionless times t for $\mathrm{El} = 3.625$ and $\mathrm{Ca} = 0.0038$. The shading in the fluid region shows the trace of the conformation tensor $\mathrm{tr}(\mathrm{A})$ which is a measure of the elastic stress. The large headed arrows make clear the flow direction inside the drop.

Although it is difficult to see from Fig. 6, the stress near the front of the drop is lower than it is towards the rear when $t = 1.3$. Consequently, the front of the drop is pulled inwards towards the rear, and this eventually forms the forward cavity shown in Fig. 5 at $t = 1.4$ and $t = 2.36$.

5 Conclusions

We have applied the volume-of-fluid (VOF) method of Rudman (1998), as extended to viscoelastic fluids by Harvie, Cooper-White and Davidson (2008), who implemented a VOF-based technique for elastic stress transport. Deformation of a viscoelastic drop in axisymmetric flow of a Newtonian fluid through a cylindrical contraction-expansion microchannel is considered. The aim is to further explore some interesting viscoelastic effects on drop deformation studied by Harvie, Cooper-White and Davidson (2008).

Harvie, Cooper-White and Davidson (2008) reported experimental results that showed the formation of a long, narrow reentrant cavity at the rear of the droplet, followed by the encapsulation of a small volume of continuous phase liquid inside the droplet. In that work, VOF simulations of two-dimensional planar flow predicted a reentrant cavity and demonstrated the role of elastic stress in the formation of the cavity and encapsulation; however, the resolution of these fine scale features was not sufficient. Rather than perform a full three-dimensional calculation at very high resolution, we have chosen instead to study drop behaviour in flow through an axisymmetric cylindrical geometry whose dimensions in its generating plane are identical to those of the previously studied planar geometry. The cylindrical geometry has a greater area contraction ratio than the planar geometry, and so will promote the growth of elastic stress, and hence cavity formation, within the droplet.

The droplet and continuous phases are taken to have the same density and viscosity as those used by Harvie, Cooper-White and Davidson (2008). Also, the capillary and elasticity numbers for the base case were chosen ($\mathrm{Ca} = 0.019$, $\mathrm{El} = 0.725$) to ensure that corresponding values, local to the contraction, are approximately the same as in Harvie, Cooper-White and Davidson (2008). The Reynolds number was fixed at $\mathrm{Re} = 1.031$. Simulations were performed for $\mathrm{El} = 0.145, 0.725, 3.625$ and $\mathrm{Ca} = 0.0038, 0.019, 0.095$.

The results show that cavity formation is promoted by reducing the capillary number. This occurs because the drop surface is then closer to the contraction wall so that frictional forces on the drop, and hence elastic stresses due to polymer stretching, are greater. Surprisingly, the effect on the rear cavity of changing the elasticity number over the range considered is small, although the effect is greatest for the lowest capillary number. An unexpected prediction is the formation of a cavity in

the forward face of the drop after it exits the contraction. This occurs at the two lowest capillary numbers ($Ca = 0.0038, 0.019$) when the elasticity number is highest ($El = 3.625$). When $Ca = 0.0038$ and $El = 3.625$, the forward cavity eventually completely penetrates the drop so that it becomes a torus. The development of the forward cavity is initiated by the high elastic stress associated with the drop fluid still within contraction acting on the drop fluid exiting the contraction. Subsequent interaction between flow and elastic stress results in the formation of a narrow band of high elastic stress along the drop centreline that pulls the front of the drop inwards to form the forward cavity. This band of elastic stress not only promotes cavity formation but also helps to stabilise the thin thread of surrounding liquid that comprises the cavity by dampening disturbances on the cavity wall.

Acknowledgement: This research was supported by the Australian Research Council Grants Scheme.

References

Aggarwal, N.; Sarkar, K. (2008): Effects of matrix viscoelasticity on viscous and viscoelastic drop deformation in a shear flow. *J. Fluid Mech.*, vol. 601, pp. 63-84.

Chung, C.; Hulsen, M. A.; Kim, J. M.; Ahn, K. H; Lee, S. J. (2008): Numerical study on the effect of viscoelasticity on drop deformation in simple shear and 5:1:5 planar contraction/expansion microchannel. *J. Non-Newtonian Fluid Mech.*, vol. 155, pp. 80-93.

Davidson, M. R.; Harvie, D. J. E.; Cooper-White, J. J. (2006): Simulations of pendant drop formation of a viscoelastic liquid. *Korea-Australia Rheology J.*, vol. 18, pp. 41-49.

Harvie, D. J. E.; Cooper-White, J. J.; Davidson, M. R. (2008): Deformation of a viscoelastic droplet passing through a microfluidic contraction. *J. Non-Newtonian Fluid Mech.*, vol. 155, pp. 67-79.

Harvie, D. J. E.; Davidson, M. R.; Cooper-White, J. J.; Rudman, M. (2006): A parametric study of droplet deformation through a microfluidic contraction: Low viscosity Newtonian droplets. *Chemical Engineering Science*, vol. 61, pp. 5149-5158.

Harvie, D. J. E.; Davidson, M. R.; Cooper-White, J. J.; Rudman, M. (2007): A parametric study of droplet deformation through a microfluidic contraction: Shear thinning liquids. *Int. J. Multiphase Flow*, vol. 33, pp. 545-556.

Keunings, R. (1986): An algorithm for the simulation of transient viscoelastic flows with free surfaces. *J. Comput. Physics*, vol. 62, pp. 199-220.

Khismatullin, D.; Renardy, Y.; Renardy, M. (2006): Development and implementation of VOF-PROST for 3D viscoelastic liquid-liquid simulations. *J. Non-Newtonian Fluid Mech.*, vol. 140, pp. 120-131.

Pillapakkam, S. B.; Singh, P. (2001): A level-set method for computing solutions to viscoelastic two-phase flow. *J. Comput. Physics*, vol. 174, pp. 552-578.

Ramaswamy, S.; Leal, L.G. (1999): The deformation of a viscoelastic drop subjected to steady uniaxial extensional flow of a Newtonian fluid. *J. Non-Newtonian Fluid Mech.*, vol. 85, pp. 127-163.

Rudman, M. (1998): A volume tracking method for intercfacial flows with large density variations. *Int. J. Numer. Methods in Fluids*, vol. 28, pp. 357-378.

Tome, M. F.; Doricio, J. L.; Castelo, A.; Cuminato, J. A.; McKee, S. (2007a): Solving viscoelastic free surface flows of a second order fluid using a marker-and-cell approach. *Int. J. Numer. Methods in Fluids*, vol. 53, pp. 599-627.

Tome, M. F.; Grossi, L.; Castelo, A.; Cuminato, J. A.; McKee, S.; Walters, K. (2007b): Die-swell, splashing drop and a numerical technique for solving the Oldroyd-B model for axisymmetric free surface flows. *J. Non-Newtonian Fluid Mech.*, vol. 141, pp. 148-166.

Verhulst, K.; Cardinaels, R.; Moldenaers, P.; Renardy, Y.; Afkhami, S. (2009): Influence of viscoelasticity on drop deformation and orientation in shear flow Part 1. Stationary states. *J. Non-Newtonian Fluid Mech.*, vol. 156, pp. 29-43.

You, R.; Borhan, A.; Haj-Hariri, H. (2008): A finite volume formulation for simulating drop motion in a viscoelastic two-phase system. *J. Non-Newtonian Fluid Mech.*, vol. 153, pp. 109-129.

Zhou, C.; Yue, P.; Feng, J. J.; Ollivier-Gooch, C.F.; Hu, H.H. (2010): 3D phase-field simulations of interfacial dynamics in Newtonian and viscoelastic fluids. *J. Comput. Physics*, vol. 229, pp. 498-511.